Corrosion Science 215 (2023) 111025

Contents lists available at ScienceDirect

Corrosion Science

journal homepage: www.elsevier.com/locate/corsci

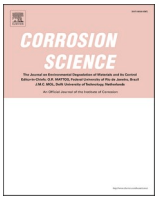

Experimental comparison of gaseous and electrochemical hydrogen charging in X65 pipeline steel using the permeation technique

Erik Koren [a,*], Catalina M. H. Hagen [b], Dong Wang [a], Xu Lu [a], Roy Johnsen [a], Junichiro Yamabe [c]

[a] Department of Mechanical and Industrial Engineering, NTNU, 7491 Trondheim, Norway
[b] SINTEF, Richard Birkelandsvei 2B, 7465 Trondheim, Norway
[c] Department of Mechanical Engineering, Fukuoka University, 8-19-1 Nanakuma, Jonan-ku, Fukuoka 814-0180, Japan

ARTICLE INFO

Keywords:
A. Low alloy steel
B. Hydrogen permeation
B. Galvanostatic
C. Hydrogen embrittlement
C. Hydrogen absorption

ABSTRACT

Herein, hydrogen uptake and diffusivity in X65 pipeline steel were investigated using the permeation technique under different hydrogen charging conditions. Hydrogen charging was performed using hydrogen gas at different pressures, and electrochemical charging was performed at different cathodic current densities. The results revealed that both the sub-surface hydrogen concentration in lattice and reversible trap sites and the effective hydrogen diffusivity were dependent on the charging conditions. Moreover, the relationship between equivalent hydrogen fugacity and overpotential was determined.

1. Introduction

The world is going through a transition from using fossil fuels towards using more renewable energy sources, aiming to reduce the emission of greenhouse gases. Hydrogen, as a clean energy carrier, is regarded as a key building block in realising a climate-neutral and zero-pollution economy [1]. For long-distance transportation of hydrogen gas, pipelines are an economically favoured choice [2,3]. A reassignment of the existing infrastructure of steel pipelines utilised for transportation of natural gas, to transport hydrogen gas, could reduce hydrogen delivery costs by 60% [4] and ease the realisation of a hydrogen economy.

However, thorough material investigations are required for safe transportation of hydrogen gas via steel pipelines. Atomic hydrogen can absorb and diffuse into steel and potentially degrade its mechanical properties; this phenomenon is referred to as hydrogen embrittlement (HE) [5–8]. Although, tensile and fatigue investigations in gaseous hydrogen environment have shown a decrease in ductility and increased fatigue crack growth rate [6,9–16], the majority of hydrogen-related studies have been performed using electrochemical charging. One reason for this is that gaseous hydrogen charging facilities are limited and mandate strict safety protocols [17]. To compare investigations of HE susceptibility utilising electrochemical and gaseous charging, the charging methods should produce a comparable hydrogen concentration, as the concentration of hydrogen in steel can affect the degree of HE [6,12,18]. Therefore, the establishment of a relationship between the severity of hydrogen gas charging and electrochemical charging is critical.

It has been proposed that two charging conditions are equivalent if they produce the same activity of hydrogen in a steel [19]. Fugacity can be regarded as the activity of a real gas; hence, the hydrogen fugacity, f_{H_2}, relates to the ease of hydrogen uptake at the surface of a specific metal [19–21]. Studies correlating electrochemical charging and hydrogen gas charging have determined the equivalent hydrogen fugacity, $f_{H_2}^{eq}$, during electrochemical charging. $f_{H_2}^{eq}$ is typically expressed as a function of the overpotential, η. The hydrogen permeation technique [18,19] and thermal desorption spectroscopy (TDS) [21–23] are the two methods employed to determine $f_{H_2}^{eq}$. In a permeation cell, hydrogen enters the sample membrane on one side (charging side), diffuses through the sample membrane, and is oxidized on the exit side (detection side) [24]. The oxidation current density or permeation current density, i_p, is a measure of the hydrogen flux passing through the sample. Fick's laws of diffusion can be used to determine the hydrogen uptake and diffusivity. Permeation tests have been used to determine $f_{H_2}^{eq}$ by comparing the permeability coefficient obtained with gas charging with that obtained using electrochemical charging [25], or to determine $f_{H_2}^{eq}$ as a function of η using electrochemical permeation in combination with thermodynamic calculations [18,19]. TDS allows the determination of the hydrogen uptake and diffusivity by measuring the amount of desorbed hydrogen gas from a precharged sample [26,27]. The

* Corresponding author.
E-mail address: erik.a.koren@ntnu.no (E. Koren).

https://doi.org/10.1016/j.corsci.2023.111025
Received 20 September 2022; Received in revised form 3 January 2023; Accepted 2 February 2023
Available online 10 February 2023

relationship between $f_{H_2}^{eq}$ and η is determined using TDS by comparing the hydrogen concentration in gas-charged and electrochemically charged samples [21–23].

However, several experimental difficulties must be overcome during charging to determine the correct value of $f_{H_2}^{eq}$. One such challenge is to maintain stable surface conditions during charging, which is an essential requirement for determining the uptake and diffusivity through the permeation technique. During electrochemical charging presence and modifications of an oxide layer, formation of corrosion products or excessive evolution of hydrogen bubbles can affect i_p [28–30]. Moreover, it has been reported that severe hydrogen charging can induce damage, such as blisters and cracks [30–33]. In gas-phase charging, a Pd coating may be necessary to achieve equilibrium on the charging side because air-formed oxides impede hydrogen entry [25,27,34]. The sub-surface lattice hydrogen concentration, C_0, has been regarded as a direct reflection of the severity of the charging condition and suggested to be an appropriate measure for comparing the uptake from different hydrogen sources [7]. However, trapping sites, which are microstructural features wherein hydrogen may reside, affect the uptake and diffusivity of hydrogen [35] rendering it difficult to determine C_0 [36]. At such trap sites, the activation energy of a hydrogen atom jumping to a neighbouring lattice site is greater than that between regular lattice sites, thus causing a reduction in the diffusivity. The term "reversible trap" typically refers to trap sites wherein hydrogen has a short residence time at the temperature of interest corresponding to a low de-trapping activation energy, whereas the term "irreversible trap" refers to trap sites where the probability of releasing trapped hydrogen is negligible under the same conditions [37]. When reversible trapping affects the transport of hydrogen in steels, the diffusion coefficient determined from permeation tests is an effective value, denoted as D_{eff}, and the sub-surface concentration includes hydrogen in lattice and reversible trap sites, denoted as C_{0R} [36]. However, if the fraction of occupied traps changes to an extent such that the permeation transient does not follow Fick's 2nd law, D_{eff} has no theoretical basis [36,38,39]. In this case, D_{eff} can vary by one order of magnitude depending on the severity of charging conditions, and C_{0R} is typically overestimated [35,40]. The change in trap occupancy can be minimized by performing successive transients with a partial increase or decrease in the charging current [41–43]. Previous reports have stated that during partial permeation transients, surface and trapping effects can be eliminated to an extent such that the lattice diffusion coefficient, D_L, can be determined [41,44].

The aim of this study was to correlate hydrogen gas charging and electrochemical charging for a X65 pipeline steel. The hydrogen uptake and diffusivity were evaluated via the permeation technique by employing both hydrogen gas charging and electrochemical charging. The dependency of D_{eff} on the charging conditions was investigated. C_{0R} was then employed to determine a relationship between $f_{H_2}^{eq}$ and η.

2. Experimental

2.1. Material and sample preparation

The material used in this study was API 5 L X65 steel from a hot-rolled and arc-welded vintage pipeline. The wall thickness was 26 mm. Its chemical composition is listed in Table 1. The samples were machined from a position close to the inner side of the pipe wall along the longitudinal direction. The samples used for the electrochemical permeation tests were disks with diameters of 30 mm and thicknesses of 1.9 mm, whereas the samples used for the gas permeation tests were 50 mm wide, 150 mm long, and 1.9 mm thick plates. Both sides of the disks and plates were ground using SiC grinding papers to a final grade of #P1000. The detection side of both types of samples were electroplated with Pd to ensure complete oxidation of hydrogen, as hydrogen oxidation is known to occur more easily on a Pd surface [45]. In addition, the plates used for gas permeation were electroplated with Pd on the charging side to overcome the surface impedance which can be caused by an oxide layer [25,27,34]. The electroplating procedure followed the method described by Husby et al. [46] based on the work of Bruzzoni et al. [47,48] and Castaño Rivera et al. [11]. After electroplating, the samples were placed in a furnace at 120 °C for 16 h to remove the hydrogen introduced during the plating process.

Table 1
Chemical composition of X65 pipeline steel.

Element	C	Si	Mn	P	S	Cu	Cr
wt%	0.1	< 0.6	< 1.6	< 0.025	< 0.015	< 0.25	< 0.25
Element	Ni	Mo	V	Nb	Ti	N	-
wt%	< 0.25	< 0.05	< 0.1	< 0.05	< 0.02	< 0.01	-

2.2. Gas permeation

A high-pressure H_2 gas permeation apparatus was employed for the tests, certified for pressures of up to 100 bar. The apparatus is illustrated in Fig. 1. H_2 gas of a 6.0 quality, with a purity of 99.9999%, was injected into the cell on the charging side from 50 L-gas bottles until a predetermined pressure was achieved. Three gas pressures, p_{H_2}, were employed for testing:10, 50, and 100 bar. The valves were then closed, and the charging of the samples commenced. The exposed surface area of the sample in each chamber was 16 cm^2. The cell corresponding to the exit side consisted of 0.1 M NaOH (pH = 12.6) with continuous N_2 gas purge. A Pt foil was used as the counter electrode. The exit surface of the Pd coated steel, was polarised at + 360 mV vs. Ag/AgCl in saturated KCl (+315 mV vs. saturated calomel electrode (SCE)) while measuring i_p. All tests were performed using succeeding transients. Three charging/discharging cycles were performed at each gas pressure. Discharging was performed by evacuating the gas on the entry side. All gas permeation tests were performed at 21 ± 1 °C.

2.3. Electrochemical permeation

An illustration of the cell used for electrochemical permeation tests is presented in Fig. 2. The sample was mounted into the sample holder and held between the two chambers in the permeation cell using gaskets and clamps. The exposed surface area of the sample in each chamber was 3.7 cm^2. The detection chamber (oxidation side) was filled with a 0.1 M NaOH electrolyte (pH = 12.6) and purged with N_2 gas. An Hg/Hg_2SO_4 electrode in saturated K_2SO_4 was used as the reference electrode, and a Pt foil was used as the counter electrode. A potential of − 80 mV vs. Hg/Hg_2SO_4 (+318 mV vs. SCE) was applied. While i_p was stabilising, the charging chamber was constantly purged with N_2 gas to avoid oxidation. When i_p attained a stable value below 0.1 μA cm^{-2}, the N_2 gas supply to the charging chamber was cut off, and a solution of 3.5 wt% NaCl (pH = 6.6) was introduced into the charging chamber. In the charging chamber, an Ag/AgCl electrode in saturated KCl was used as the reference electrode, and a Pt foil was used as the counter electrode. Different cathodic charging current densities, i_c, were applied: − 1, − 15 and − 50 mA cm^{-2}. When i_p reached a steady state, denoted as i_p^{∞}, the test was terminated, and the permeation cell was dismantled. In contrast to the gas permeation test, the sample was removed from the sample holder and kept in a desiccator overnight to allow hydrogen degassing. The charging side was further ground using a #P1000 grinding paper to remove any corrosion products within 1 h before initiation of the next transient. The change in the sample thickness was negligible. Three transients were performed for each charging condition. All electrochemical permeation tests were performed at 21 ± 1 °C.

In addition, partial permeation transients were performed to reduce trapping and potential surface effects that are known to impede hydrogen uptake [41]. First, a complete build-up permeation transient

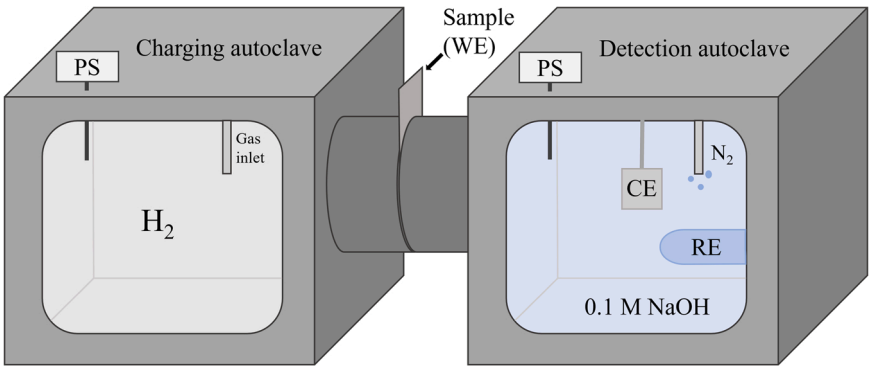

Fig. 1. Schematic of the high pressure H_2 gas permeation cell. WE – working electrode, CE – counter electrode, RE – reference electrode, PS – pressure sensor.

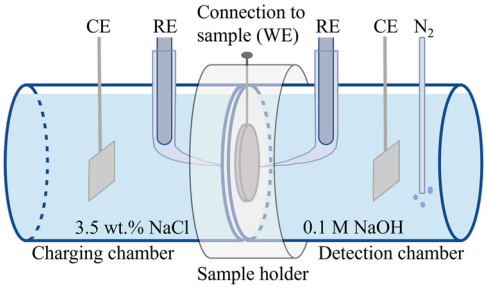

Fig. 2. Schematic of the electrochemical permeation cell. WE – working electrode, CE – counter electrode, RE – reference electrode.

was performed by applying an i_c of − 1 mA cm^{-2} for 12 h, to produce a stable surface condition. i_c was then increased in steps of 1 mA cm^{-2} in the cathodic direction until i_c reached − 7 mA cm^{-2}, while i_p was continuously measured on the detection side. A good fit between i_p and Fick's 2nd law was observed at − 7 mA cm^{-2}. After stabilisation was achieved, i_c was decreased in steps of 1 mA cm^{-2} in the anodic direction until i_c reached −1 mA cm^{-2}.

2.4. Analysis

From the permeation transients, D_{eff} can be calculated using the breakthrough time method and time lag method, as presented in Eqs. (1) and (2), respectively [24,36,38,49]. L denotes the thickness of the sample. The breakthrough time, t_b, represents the intercept between the extrapolation of the linear portion of the build-up of i_p and the baseline of i_p. A difference in t_b between the first and subsequent transients indicates irreversible trapping [37]. Irreversible traps are not emptied between successive permeation transients; hence, they slow down the hydrogen transport during the first transient but do not affect the subsequent transients. The time lag, t_{lag}, represents the time required to attain 63% of i_p^{∞}.

$$D_{eff}(t_b) = \frac{L^2}{19.8 t_b} \tag{1}$$

$$D_{eff}(t_{lag}) = \frac{L^2}{6 t_{lag}} \tag{2}$$

The diffusion coefficient of hydrogen, D, from partial permeation tests was estimated by fitting the experimental results to an analytical solution of Fick's 2nd law. The build-up of i_p can be fit to Eq. (3), and the decay of i_p can be fitted to Eq. (4) [41]. t denotes the time after changing i_c, and i_p^0 denotes the initial value of the permeation current density when i_c is changed.

$$\frac{i_p - i_p^0}{i_p^{\infty} - i_p^0} = \frac{2L}{\sqrt{\pi D t}} \sum_{n=0}^{\infty} \exp\left(-\frac{(2n+1)^2 L^2}{4Dt}\right) \tag{3}$$

$$\frac{i_p - i_p^{\infty}}{i_p^0 - i_p^{\infty}} = 1 - \frac{2L}{\sqrt{\pi D t}} \sum_{n=0}^{\infty} \exp\left(-\frac{(2n+1)^2 L^2}{4Dt}\right) \tag{4}$$

C_{0R} is proportional to i_p^{∞} and can be calculated using Eq. (5). F denotes the Faraday constant (96485 A s mol^{-1}) [36].

$$C_{0R} = \frac{i_p^{\infty} L}{F D_{eff}} \tag{5}$$

3. Results

3.1. Microstructure

Fig. 3(a) and (b) presents the scanning electron microscopy (SEM) micrographs of the studied steel. The microstructure primarily consists of polygonal ferrite, together with pearlite. The plate-like microstructure with a banded appearance indicates that some bainite is also present. The average grain size is 3.7 μm.

3.2. Hydrogen diffusivity

3.2.1. Gas permeation

Three consecutive permeation transients performed at 100 bar of H_2 gas pressures are presented in Fig. 4(a). A significant difference in t_b between the first and subsequent transients can be observed, indicating that irreversible traps affect the first transient [37]. As the investigation of irreversible traps is not within the scope of this study, the results obtained from the first transient will not be reported herein. The second and third permeation transients obtained at different p_{H_2} are presented in Fig. 4(b). Transient 2 and 3 concur well at all p_{H_2}. An increase in p_{H_2} caused an increase in i_p^{∞} and a reduction in t_b.

The normalised hydrogen flux, as a function of the normalised time for gas permeation transients, is presented in Fig. 5, along with the predictions of Fick's 2nd law calculated using the hydrogen diffusion coefficient in well-annealed bcc iron, 7.27 × 10^{-5} cm^2 s^{-1} [50]. The normalised gas permeation transients are shifted to the right and are steeper than that predicted by Fick's 2nd law. A normalised permeation transient that is steeper than that predicted by Fick's 2nd law indicates a significant change in trap occupancy, which affects the transport of hydrogen [36,38,39]. Thus, the determinations of $D_{eff}(t_b)$ and $D_{eff}(t_{lag})$ using Eqs. (1) and (2) have no theoretical basis.

The average values for D_{eff} calculated by the t_b and t_{lag} methods from transients 2 and 3 are presented in Table 2. D_{eff} increases with increasing p_{H_2}. $D_{eff}(t_b)$ ranges from 2.21 × 10^{-7} cm^2 s^{-1} at 10 bar to 3.23 × 10^{-7} cm^2 s^{-1} at 100 bar, while $D_{eff}(t_{lag})$ ranges from 4.45 × 10^{-7} cm^2 s^{-1} at 10 bar to 7.53 × 10^{-7} cm^2 s^{-1} at 100 bar. $D_{eff}(t_{lag})$ is 1.9 – 2.3 times

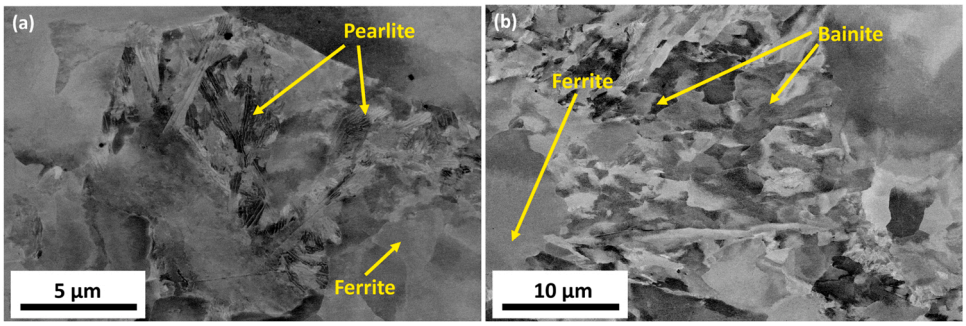

Fig. 3. SEM micrographs at (a) 5,000X and (b) 10,000X magnifications revealing the microstructure of the studied steel, which consisted of ferrite, pearlite, and bainite.

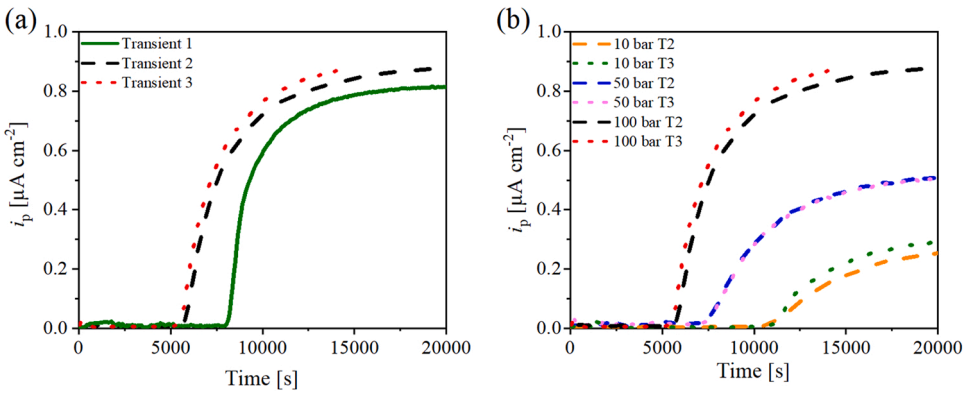

Fig. 4. (a) Three transients performed at 100 bar of hydrogen pressure. (b) Transient 2 and 3 at 10, 50, and 100 bar of hydrogen pressure. T2 – transient 2, T3 – transient 3.

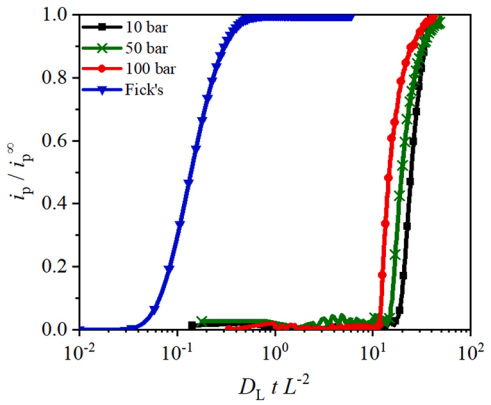

Fig. 5. Normalised gas permeation transients and prediction of Fick's 2nd law for lattice diffusion in bcc iron.

Table 2
Parameters determined by the gas permeation test. The values represent average values obtained from transients 2 and 3.

p_{H_2} [bar]	D_{eff} (t_b) [cm^2 s^{-1}]	D_{eff} (t_{lag}) [cm^2 s^{-1}]
10	$2.21 \times 10^{-7} \pm 0.01$	$4.25 \times 10^{-7} \pm 0.01$
50	$2.47 \times 10^{-7} \pm 0.01$	$5.66 \times 10^{-7} \pm 0.01$
100	$3.23 \times 10^{-7} \pm 0.03$	$7.53 \times 10^{-7} \pm 0.03$

higher than $D_{eff}(t_b)$ for all p_{H_2}, thus confirming the inference made from the normalised transients, that the effective diffusivity changes during permeation transients [35,36,38,39].

3.2.2. Electrochemical permeation

The three electrochemical permeation transients obtained at − 15 mA cm^{-2} are presented in Fig. 6(a). As was observed with gas charging, t_b of the first transient was higher than that of the subsequent transients, indicating irreversible trapping. Fig. 6(b) presents the second and third transients obtained at different levels of i_c. t_b decreases and i_p^{∞} increases with increasing i_c. Deviation between transients 2 and 3 at − 1 mA cm^{-2} and − 50 mA cm^{-2} can be observed, which indicate that the surface conditions during electrochemical charging are not as stable as those during hydrogen gas charging.

The normalised hydrogen flux, as a function of the normalised time for electrochemical permeation transients, is presented in Fig. 7, including the prediction of Fick's 2nd law, which was calculated using the lattice diffusivity of bcc iron. The trends are similar to those observed during gas charging. The normalised permeation transients are shifted toward the right and are steeper than that predicted by Fick's 2nd law.

The average values for D_{eff} determined by the t_b and t_{lag} methods for different i_c are provided in Table 3. D_{eff} increases with an increase in i_c. $D_{eff}(t_b)$ ranges from 1.95×10^{-7} to 3.61×10^{-7} cm^2 s^{-1}, while $D_{eff}(t_{lag})$ ranges from 5.24×10^{-7} cm^2 s^{-1} to 6.73×10^{-7} cm^2 s^{-1}. $D_{eff}(t_{lag})$ is 1.8 – 2.7 times higher than $D_{eff}(t_b)$ for all i_c.

3.2.3. Partial permeation transients

As the values of D_{eff} presented above appear to be significantly affected by reversible trapping, D_{eff} was determined via electrochemical partial permeation transients. The normalised partial permeation transient build-up and decay between i_c values of − 6 mA cm^{-2} and − 7 mA cm^{-2} are presented in Fig. 8(a) and (b), respectively. The best fits of the analytical solutions to Fick's 2nd law (Eqs. (3) and (4)) are included. MATLAB was used for the fitting. A good fit indicates that, in contrast to the complete permeation transient, the hydrogen diffusivity

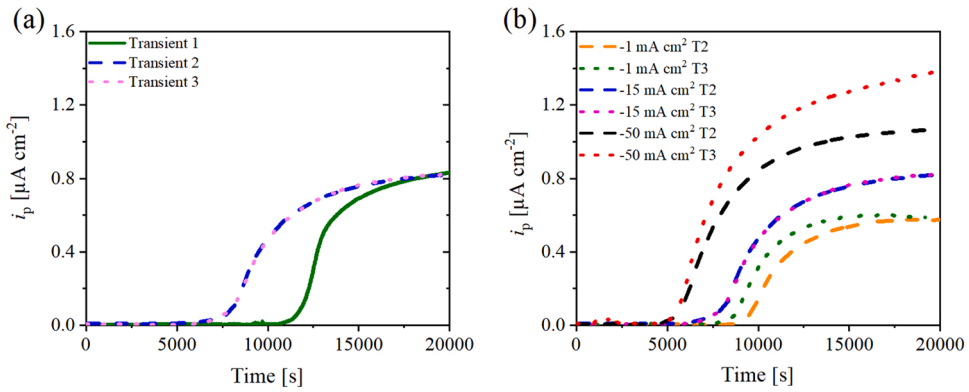

Fig. 6. (a) Three transients performed at a charging current density of − 15 mA cm^{-2} charging current density during the electrochemical permeation test. (b) Transients 2 and 3 performed at − 1, − 15 and − 50 mA cm^{-2}. T2 – transient 2, T3 – transient 3.

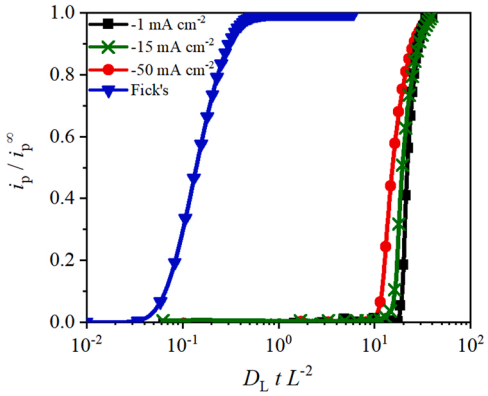

Fig. 7. Normalised electrochemical permeation transients and prediction of Fick's 2nd law for lattice diffusion in bcc iron.

Table 3
Average values for D_{eff}, as determined by the electrochemical permeation test.

i_c [mA cm^{-2}]	D_{eff} (t_b) [cm^2 s^{-1}]	D_{eff} (t_{lag}) [cm^2 s^{-1}]
-1	$1.95 \times 10^{-7} \pm 0.08$	$5.24 \times 10^{-7} \pm 0.23$
-15	$2.22 \times 10^{-7} \pm 0.01$	$5.43 \times 10^{-7} \pm 0.01$
-50	$3.61 \times 10^{-7} \pm 0.45$	$6.73 \times 10^{-7} \pm 0.09$

between the aforementioned two charging conditions can be represented by Fick's 2nd law [41,43]. The best fit of D_{eff} to the build-up curve is 1.68×10^{-6} cm^2 s^{-1}, while the best fit to the decay curve is 1.55×10^{-6} cm^2 s^{-1}. An average value of 1.6×10^{-6} cm^2 s^{-1} is denoted as D_{eff}(PT).

3.3. Hydrogen uptake

3.3.1. Uptake from gas permeation

C_{0R} values at different p_{H_2} obtained from different calculation methods are presented in Table 4. These values depend on the calculation method. D_{eff} changes during complete permeation transients; hence, the $C_{0R}(t_b)$ and $C_{0R}(t_{lag})$ values appear different. The $C_{0R}(t_b)$ values are 1.9 – 2.3 times higher than the $C_{0R}(t_{lag})$ values for all p_{H_2}.During stepwise charging, the partial transients could be fitted to Fick's 2nd law. Thus, it can be argued that the value of C_{0R} calculated from Eq. (5) using i_p^∞ from the complete permeation transient and D_{eff}(PT) represents the best measure of C_{0R} and is denoted as C_{0R}(PT). At p_{H_2} of 10, 50, and 100 bar, C_{0R}(PT) was 0.047, 0.082 and 0.137 wppm,

Table 4
C_{0R} determined by different methods from gas permeation. The values represent average values of transients 2 and 3.

p_{H_2} [bar]	f_{H_2} [bar]	C_{0R} (t_b) [wppm]	C_{0R} (t_{lag}) [wppm]	C_{0R} (PT) [wppm]
10	10.1	0.341 ± 0.011	0.183 ± 0.001	0.047 ± 0.002
50	51.6	0.529 ± 0.002	0.231 ± 0.001	0.082 ± 0.000
100	106.7	0.681 ± 0.011	0.295 ± 0.001	0.137 ± 0.002

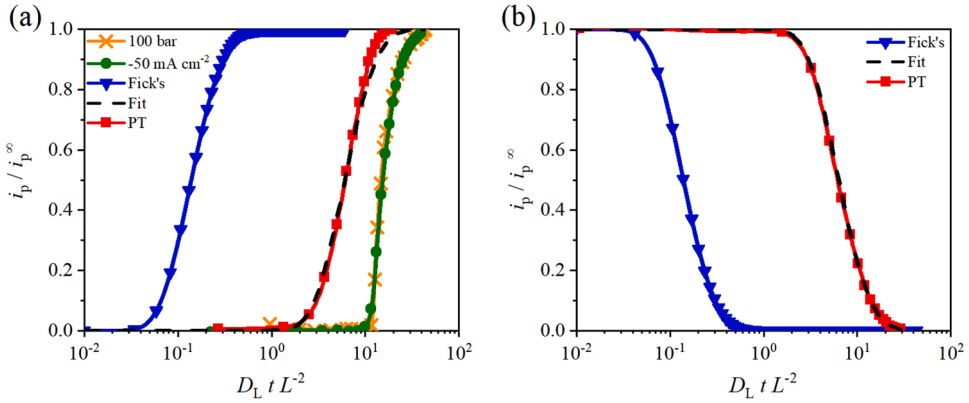

Fig. 8. (a) Normalised build-up partial permeation transients from − 6 mA cm^{-2} to − 7 mA cm^{-2} with best the fit to Eq. (3). Normalised transients at one hundred bar, − 50 mA cm^{-2} and a prediction of Fick's 2nd law for lattice diffusion in bcc iron are included for comparison. (b) Normalised decay permeation transients from − 7 mA cm^{-2} to − 6 mA cm^{-2} with the best fit to Eq. (4). PT – partial transient.

respectively. Sieverts' law, Eq. (6), states that the concentration of dissolved hydrogen in a metal is proportional to the square root of f_{H_2} in a charging atmosphere [51]. At a steady-state, C_0 is proportional to C_{0R} [52]; thus, Sieverts' law is also valid for C_{0R}. The hydrogen fugacity can be calculated from the hydrogen partial pressure using the Able-Noble equation of state, Eq. (7), where b denotes a constant (1.584×10^{-5} m^3 mol^{-1}), T denotes the temperature in K, and R denotes the gas constant (8.314 J K^{-1} mol^{-1}) [20]. The linearity between C_{0R} and $f_{H_2}^{1/2}$, observed in Fig. 9, is in agreement with Sieverts' law. Sieverts' constant, S, determined from the linear regression line, has a value of 0.0125 wppm $bar^{-1/2}$.

$$C_0 = S \times \sqrt{f_{H_2}} \tag{6}$$

$$f_{H_2} = p_{H_2} \exp\left(\frac{p_{H_2} b}{RT}\right) \tag{7}$$

3.3.2. Uptake from electrochemical permeation

C_{0R} values at different i_c obtained from different calculation methods are listed in Table 5. As was observed with gas charging, C_{0R} values appear to be dependent on the calculation method. $C_{0R}(t_b)$ values are 1.9 – 2.7 times higher than $C_{0R}(t_{lag})$ values for all i_c. Additionally, the $C_{0R}(t_b)$ values are 4.6–8.2 times higher than C_{0R}(PT), and the $C_{0R}(t_{lag})$ values are 2.3–3.1 times higher than C_{0R}(PT). At − 1, − 15, and − 50 mA cm^{-2}, C_{0R}(PT) is 0.090, 0.129, and 0.189 wppm, respectively. C_{0R}(PT) is proportional to $i_c^{1/2}$, as presented in Fig. 10.

3.3.3. Equivalent fugacity

$f_{H_2}^{eq}$ was determined using the method described by Venezuela et al. [21,22] and Liu et al. [23]. The values of C_{0R}(PT) determined from electrochemical charging were inserted into Eq. (6), and the equation was solved for f_{H_2} to determine $f_{H_2}^{eq}$. S determined from gas charging, 0.0125 ppm $bar^{-1/2}$, was used in the calculations. Fig. 11 presents the C_{0R}(PT) values determined from electrochemical charging superimposed onto the linear regression line corresponding to Sieverts' law. The equivalent hydrogen charging pressure, $p_{H_2}^{eq}$, was determined by solving Eq. (7) iteratively using the Newton-Raphson method. The values of $f_{H_2}^{eq}$ and $p_{H_2}^{eq}$ are listed in Table 6. i_c values of − 1, − 15, and − 50 mA cm^{-2} correspond to $f_{H_2}^{eq}$ values of 49.1, 101.9, and 222.7 bar, respectively.

The value of η is determined using Eq. (8). E_c denotes the average measured potential on the charging side, and E_H^0 denotes the equilibrium potential for a hydrogen evolution reaction in solution under standard state conditions, as described by Eq. (9) [19,53]. The average measure η at − 1, − 15 and − 50 mA cm^{-2} was − 593 ± 3, − 1133 ± 23, and − 2023 ± 74 mV, respectively.

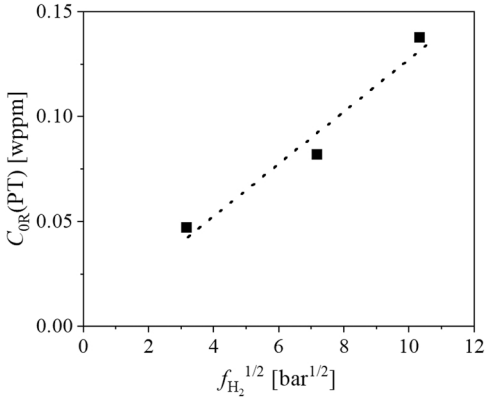

Fig. 9. Sub-surface hydrogen concentration C_{0R}(PT) versus the square root of hydrogen charging fugacity.

Table 5
C_{0R} values determined by different methods from electrochemical permeation. The values represent averages values of transients 2 and 3.

i_c [mA cm^{-2}]	C_{0R} (t_b) [wppm]	C_{0R} (t_{lag}) [wppm]	C_{0R} (PT) [wppm]
− 1	0.740 ± 0.016	0.276 ± 0.007	0.090 ± 0.002
− 15	0.929 ± 0.011	0.370 ± 0.007	0.129 ± 0.001
− 50	0.864 ± 0.219	0.450 ± 0.065	0.189 ± 0.025

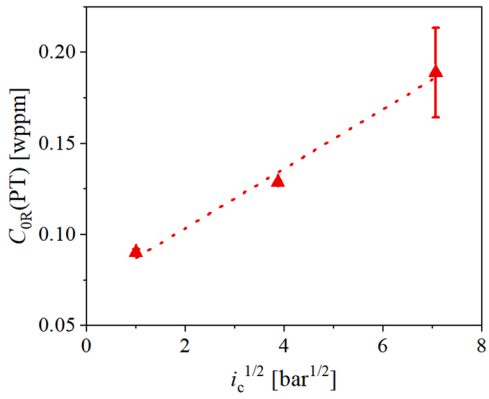

Fig. 10. Sub-surface hydrogen concentration C_{0R}(PT) versus the square root of charging current density.

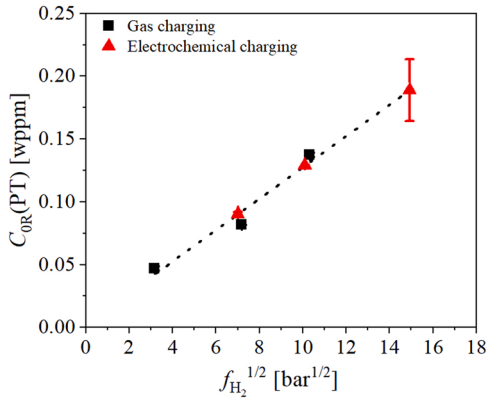

Fig. 11. Sub-surface hydrogen concentration C_{0R}(PT) versus the square root of the hydrogen fugacity along with values obtained from electrochemical charging superimposed onto the best linear fit of gaseous charging.

Table 6
Equivalent hydrogen pressure and equivalent hydrogen fugacity.

i_c [mA cm^{-2}]	C_{0R} (PT) [wppm]	$p_{H_2}^{eq}$ [bar]	$f_{H_2}^{eq}$ [bar]
− 1	0.090 ± 0.002	47.6	49.1
− 15	0.129 ± 0.001	95.9	101.9
− 50	0.189 ± 0.025	196.4	222.7

$$\eta = E_c - E_H^0 \tag{8}$$

$$E_H^0 = -0.0591 \times \mathrm{pH} - 0.0295 \log f_{H_2} \tag{9}$$

The mathematical relationship between $f_{H_2}^{eq}$ and η was determined using the approach described by Atrens et al. [18] and Liu et al. [19]. Thorough analyses of the development of a mathematical expression for the relationship between $f_{H_2}^{eq}$ and η during electrochemical permeation tests can be found elsewhere [18,19,54,55]. In short, the Nernst equation can be used to relate $f_{H_2}^{eq}$ to η, as indicated in Eq. (10). A and ξ denote

parameters that can be determined experimentally using the relations provided in Eqs. (11) and (12), respectively.

$$f_{H_2}^{eq} = A\exp\left(\frac{-\eta F}{\xi RT}\right) \tag{10}$$

$$\xi = -\frac{1}{2}\frac{F}{R\,T}\frac{\delta\eta}{\delta \ln i_p^{\infty}} \tag{11}$$

$$i_p^{\infty} = \frac{FDS}{L}\left(A\exp\left(-\frac{\eta F}{\xi RT}\right)\right)^{1/2} \tag{12}$$

The constants ξ and A, as well as D_{eff}(PT) and S determined in this study, were substituted into Eq. (10). The mathematical relation between the $f_{H_2}^{eq}$ and η is described by Eq. (13). It should be emphasized that galvanostatic charging was used in this study, and η was determined from the average potential measured during the transients.

$$f_{H_2}^{eq} = 32.19\exp\left(-\frac{\eta F}{38.81RT}\right) \tag{13}$$

4. Discussion

The aim of this study was to determine the relationship between hydrogen gas charging and electrochemical charging. $f_{H_2}^{eq}$ was determined as a function of η under the assumption that different charging conditions producing equal concentrations of hydrogen in steel are equivalent. To compare the severity of electrochemical and gaseous hydrogen charging conditions based on the hydrogen permeation technique, it is necessary to have an accurate measure of the sub-surface hydrogen concentration. Because the calculation of C_{0R} depends on D_{eff}, it is important to carefully evaluate D_{eff}. Detailed discussions on hydrogen diffusion and uptake are presented in the following sections.

4.1. Hydrogen diffusivity

The normalised permeation transients (Figs. 5 and 7) were shifted to the right and steeper than predicted by Fick's 2nd law. A normalised transient that is shifted to the right along the x-axis indicates slower diffusion than lattice diffusion, while a slope that deviates from Fick's 2nd law indicates that the diffusion coefficient appears to increase during the transient due to significant reversible trapping (steeper slope) or that the surface conditions are unsteady (less steep slope) [36,38,39]. Hence, the observed effects on the normalised transients reveal that a significant change in reversible trap occupancy affected both the electrochemical and gaseous permeation transients. It was also evident from the difference between $D_{eff}(t_b)$ and $D_{eff}(t_{lag})$ that significant trap occupancy caused D_{eff} to change during the permeation transients. For all tests, the value of $D_{eff}(t_b)$ was smaller than $D_{eff}(t_{lag})$. Hence, the probability of diffusing hydrogen being trapped is lowest at t_{lag}, and the effective diffusivity appears faster [7]. Because D_{eff} appears to change during a transient, it does not have a theoretical basis in Fick's 2nd law [36,38,39].

Essentially, t_b should be independent of the magnitude of the hydrogen flux through a sample [56]. However, it is evident from Figs. 4(b) and 6(b) that t_b decreases with increasing p_{H_2} and i_c. A decrease in t_b with an increase in i_c has been previously reported [30,49]. The reduced value of t_b is attributed to a higher flux of hydrogen diffusing through the material, which causes traps to be occupied at a faster rate. Thus, the impediment to hydrogen transport caused by traps is more pronounced when the hydrogen flux is low. It is evident from Tables 2 and 3 that the D_{eff} values are dependent on the charging conditions. Fig. 12 presents D_{eff} values as a function of i_p^{∞}. A similar relationship between C_0 and D_{eff} was predicted by Griffiths and Turnbull [35] using theoretical calculations based on electrochemical permeation results obtained from three low alloy steels. C_0 is proportional to i_p^{∞}; thus, it is expected that the dependency of D_{eff} on the concentration follows the same trend. D_{eff} obtained from gaseous charging is slightly larger than those obtained from electrochemical charging for the same value of i_p^{∞}. A possible explanation is the smaller radius to thickness ratio (5:1) during electrochemical permeation, compared to that during gaseous permeation (10:1). A smaller radius to thickness ratio can cause deviation from the assumption of one-dimensional diffusion due to increasing influence of lateral diffusion. According to the study by Hutchings et al. [57], a radius to thickness ratio of 10:1 and 5:1 can cause a deviation of less than 5% and about 10%, respectively, when one-dimensional diffusion is assumed. Owing to the concentration dependency of D_{eff}, the effective diffusivity should not be treated as an intrinsic material property unless the trap occupancy is very low [7]. The concentration dependence of the effective diffusivity underlines the importance of performing tests in charging conditions comparable to the operating conditions.

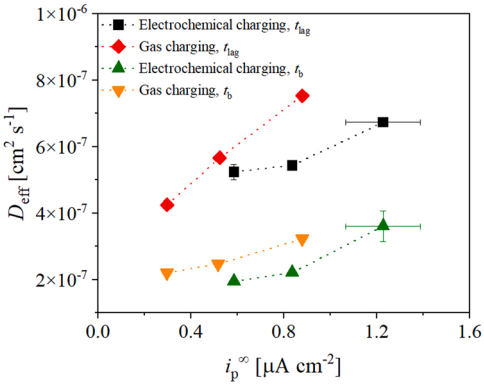

Fig. 12. Effective diffusion coefficients, $D_{eff}(t_b)$ and $D_{eff}(t_{lag})$, as a function of the steady-state permeation current density, i_p^{∞}.

Because $D_{eff}(t_b)$ and $D_{eff}(t_{lag})$ were significantly affected by the change in trap occupancy, partial permeation transients were performed. This approach caused a smaller disturbance to the equilibrium between the lattice and trapped hydrogen, that is, the change in the trap occupancy was small [41]. This method could, as reported in the literature, be used to determine D_L of hydrogen in bcc iron [41]. Partial permeation transients have also been applied to X65 low alloy steels, where the reported value of D_L is in the order of 1–3 × 10^{-6} cm^2 s^{-1} [44]. The diffusion coefficient determined by the partial transient in this study was approximately 1.6 × 10^{-6} cm^2 s^{-1}, with the same order of magnitude as that reported for X65 low alloy steel. However, even with a minimal change in trap occupancy, the effect of reversible traps was not completely eliminated in this study. Thus, the diffusion coefficient obtained from the partial transients was regarded as an effective value. However, D_{eff}(PT) is in this case regarded as the best measure of hydrogen diffusivity in steady-state conditions.

4.2. Hydrogen uptake

Two charging conditions resulting in the same hydrogen activity below the steel surface are considered to be equivalent [19]. As explained above, the complete permeation transients could not be fit to Fick's 2nd law; thus, the determination of $C_{0R}(t_b)$ and $C_{0R}(t_{lag})$ does not have a theoretical basis. In such a case, C_{0R} obtained from the t_b and t_{lag} methods can be overestimated by a factor of 2.5–5 [40]. As observed in Fig. 8(a) and (b), the effects produced by changes in trap occupancy are reduced when performing partial permeation transients to an extent such that the transients agree well with Fick's 2nd law. D_{eff}(PT) obtained from partial transients and i_p^{∞} obtained from the complete permeation transient were used to calculate C_{0R}(PT) using Eq. (5). As D_{eff}(PT) was considered the best measure of hydrogen diffusivity in a steady-state, C_{0R}(PT) was used to determine $f_{H_2}^{eq}$. It has been argued that C_0 is the best measure of the severity of charging conditions [7]. To determine C_0,

it is often considered that the hydrogen flux in a steady-state is equal to the lattice hydrogen flux and D_L in bcc iron is substituted into Eq. (5). In this study, reversible trapping was so significant that this assumption was not made. However, because a single value of D_{eff} is used to determine C_{0R}(PT), whether C_0 or C_{0R}(PT) forms the basis for comparison does not affect the relationship between $f_{H_2}^{eq}$ and η.

The determination of $f_{H_2}^{eq}$ as a function of η by hydrogen permeation requires the following conditions to be satisfied: (i) Sieverts' law must apply to both gas charging and electrochemical charging, (ii) equilibrium conditions must exist on the charging side, and (iii) the permeation transients must be described by Fick's 2nd law [19]. The linearity of C_{0R} with both $p_{H_2}^{1/2}$ and $i_c^{1/2}$ indicates that Sieverts' law applies to both electrochemical and gas charging. The linear dependence between C_{0R} and $i_c^{1/2}$, as presented in Fig. 10, is attributed to the balance between charging and chemical recombination [52]. Equilibrium conditions on the charging side were obtained by eliminating surface effects that impeded hydrogen uptake. During gas charging, a Pd coating was applied to the charging side, as air-formed surface oxides can cause surface impedance to hydrogen uptake from hydrogen gas [27,34]. Pd coatings have been reported to eliminate the impeding effect of surface oxides and ensure equilibrium between the gas and metal phases, according to Sieverts' law [11,25,27,34]. However, a few studies on hydrogen gas permeation have not mentioned the use of Pd coatings on the charging side [9,10,58]. The linear dependence between C_{0R}(PT) and $p_{H_2}^{1/2}$ with an intercept close to the origin indicates that the Pd coating ensure equilibrium conditions on the charging side and that the Pd coated surface represents the hydrogen uptake of a bare steel surface (for instance in a growing crack tip).

During electrochemical hydrogen permeation, the second and third permeation transients were less coincident (Fig. 6(b)) than those of gas charging (Fig. 4(b)), especially when charging at − 50 mA cm^{-2}. This indicated that the surface conditions were less stable during electrochemical charging. One possible explanation for this is that the surface conditions were slightly different between the transients, as the sample was removed from the cell and ground, which was not the case for gas charging. The largest deviation between transients 2 and 3 was observed during charging at − 50 mA cm^{-2}. Corrosion has been reported to take place under high cathodic current densities, possibly due to extensive evolution of hydrogen bubbles disturbing local electrochemical conditions [29,30]. Air-formed oxides could impede hydrogen uptake also during electrochemical charging; however, it has been reported that the oxides can be reduced during the early stage of hydrogen permeation on the order of minutes to one hour in NaOH solution [28,29]. If this were the case here, the air-formed oxide would be reduced faster than t_b such that the removal of surface oxides could affect the shape of the transient without affecting i_p^{∞}. If the shape of the electrochemical transient was affected by an air-formed oxide, it can be an additional explanation to why D_{eff} is slightly smaller for electrochemical permeation than for gas permeation at equal i_p^{∞}, as observed in Fig. 12. In addition, blisters and surface cracks can be formed under severe charging conditions but are more likely to form in acidic solutions with added hydrogen recombination poisons [31,32]. The linear dependence of C_{0R}(PT) on $i_c^{1/2}$ indicated equilibrium conditions on the charging side. Combined with the partial transients following Fick's 2nd law, conditions (i), (ii), and (iii) were considered as satisfied.

An advantage of determining $f_{H_2}^{eq}$ using both gas charging and electrochemical permeation is that through gas charging, one can determine S for the specific material investigated. S is necessary to determine $f_{H_2}^{eq}$ as a function of η using Eq. (10), and a difference in S can significantly affect the relationship between $f_{H_2}^{eq}$ and η determined by electrochemical hydrogen permeation. S of pure bcc iron is approximately 5.3×10^{-4} wppm bar$^{-1/2}$ [19,50], which is approximately two orders of magnitude lower than the value obtained in this study. For a 3.5NiCrMoV steel specimen, S was reported to be 0.0272 wppm bar$^{-1/2}$ [22], which is approximately twice the value determined in this study. In materials with low solubility and high diffusivity, such as low carbon steels, it can be challenging to conduct accurate measurements with TDS. A substantial amount of hydrogen can egress between hydrogen charging and analysis, and it may be necessary to estimate the amount of effused hydrogen during this dwell time [22,59]. Using the permeation technique, small fluxes of hydrogen can be detected simultaneously with hydrogen exposure on the charging side, rendering this an advantageous method for samples with low solubility and high diffusivity.

A summary of previous studies including the current study, which determined $f_{H_2}^{eq}$ as a function of η, is presented in Fig. 13 [19,21,23,54,60]. The plot illustrates different charging methods that can represent equal hydrogen activities. However, the relationship between $f_{H_2}^{eq}$ and η is, to a large extent, specific to the electrolyte and the investigated alloy owing to the variation in the microstructure and surface conditions that affect hydrogen evolution [21]. This is further demonstrated by comparing the results of this study with the values obtained by Venezuela et al. [21] for a martensitic advanced high-strength steel, which was also charged in a 3.5 wt% NaCl solution and obtained a similar magnitude of $f_{H_2}^{eq}$ but at a lower η. The results obtained Liu et al. [23] for a dual phase steel in 3 wt% NaCl are comparable to that obtained by Venezuela et al. [21], both studies using a TDS based approach. Crolet and Maisonneuve [60] obtained a lower $f_{H_2}^{eq}$, when charging a low carbon steel walled hollow sensor in a 5 wt% NaCl solution, compared to the other studies that performed charging in NaCl solutions. A change in the slope was observed in results of certain studies presented in Fig. 13, which was attributed to a change in the hydrogen evolution reaction mechanism [19,54]. This change in the slope was not observed in this study; however, it may occur outside the tested range of η. A change in the slope at lower η could bring the $f_{H_2}^{eq}$ closer to the value obtained by Crolet and Maisonneuve. As a change in the slope may occur outside the tested range of η, the relationship between $f_{H_2}^{eq}$ and η may not be valid outside the investigated range.

The determined relationship between $f_{H_2}^{eq}$ and η for the investigated steel specimen (Eqs. (6) and (13)) is related to the hydrogen uptake of bare metal surface, as the influence of an oxide layer is eliminated by using a Pd-coated surface during gas charging. The nature of failure can make it difficult to make direct comparisons between investigations of HE susceptibility performed with different charging methods [6]; thus,

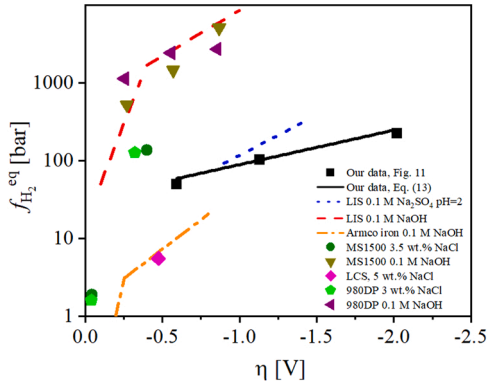

Fig. 13. Equivalent fugacity, $f_{H_2}^{eq}$, versus overpotential, η. Included data: Study conducted by Liu et al. [19] on low interstitial steel (LIS) charged in both 0.1 M NaOH and acidified 0.1 M Na_2SO_4 (pH = 2) in permeation tests; Study conducted by Venezuela et al. [21] on MS1500 martensitic advanced high-strength steels charged in 0.1 M NaOH and 3.5 wt% NaCl; Study conducted by Liu et al. [23] on 98DP dual phase steels charged in 0.1 M NaOH and 3 wt% NaCl;Study conducted by Crolet and Maisonneuve [60] on low carbon steel (LCS) in 5 wt% NaCl; Data collected by Bockris et al. [54] on Armco iron in 0.1 M NaOH with the relationship deduced by Liu et al. [19].

the determined equivalency between charging methods and hydrogen uptake may not translate to mechanical testing. Validation of equivalence between charging methods and hydrogen uptake using mechanical testing requires thorough design. For instance, during HE investigation by mechanical testing, hydrogen uptake between gaseous and electrochemical charging at equivalent fugacity may differ initially due to the surface impedance of the oxide layer. However, strain will cause breakage of the oxide film [6], which will expose the bare steel surface to the hydrogen gas and uptake will proceed according to Sieverts' law. Surface oxides prepared on a steel surface can inhibit hydrogen uptake, however, the efficiency is dependent on the nature of the oxide film as hydrogen uptake take place through pores and cracks [10]. Similarly, naturally formed oxide layers present during in-service conditions may act as a barrier to hydrogen uptake. Thus, further work is necessary to investigate the equivalency between investigations of HE susceptibility using different charging methods, and hydrogen uptake under in-service conditions.

5. Conclusion

In this study, the hydrogen permeation technique was used to investigate the hydrogen uptake and diffusivity under different charging conditions. Electrochemical and gaseous hydrogen charging were conducted. The sub-surface hydrogen concentration in lattice and reversible trap sites were used to compare the severity of the charging conditions, and to determine the relationship between the equivalent hydrogen fugacity and overpotential. Additionally, the dependence of the effective diffusivity of hydrogen on the charging conditions was investigated. Partial permeation transients were performed to reduce the effect of trapping on permeation transients. The primary findings are summarised as follows:

- The sub-surface hydrogen concentration in lattice and reversible trap sites, C_{0R}, increased linearly with the square root of both the hydrogen gas charging fugacity and charging current density.
- The effective diffusion coefficient, D_{eff}, determined via the breakthrough time method and the time lag method was dependent on the charging conditions owing to significant reversible trapping. Its values were found to lie in the range of 2–8 $\times$ 10^{-7} cm^2 s^{-1} at room temperature. Performing partial permeation transients reduced the effects produced by changes in trap occupancy to the extent that the permeation transients followed Fick's 2nd law. The value of D_{eff} determined by partial permeation transients was in the order of 1.6 $\times$ 10^{-6} cm^2 s^{-1} at room temperature.
- A relationship between the equivalent hydrogen fugacity and overpotential was deduced. During gaseous hydrogen charging, a Pd coating was utilised to overcome the surface impedance which can be caused by an oxide layer. Further work is necessary to investigate the equivalence of charging methods during mechanical testing, and hydrogen uptake from hydrogen gas where naturally formed surface oxides are present.

CRediT authorship contribution statement

Erik Koren: Conceptualization, Methodology, Formal analysis, Investigation, Data curation, Writing – original draft. **Catalina Hoem Musinoi Hagen:** Conceptualization, Methodology, Investigation, Writing – review & editing. **Dong Wang**: Supervision, Investigation, Writing – review & editing. **Xu Lu**: Conceptualization, Writing – review & editing. **Roy Johnsen**: Supervision, Conceptualization, Writing – review & editing. **Junichiro Yamabe:** Conceptualization, Writing – review & editing.

Declaration of Competing Interest

The authors declare that they have no known competing financial interests or personal relationships that could have appeared to influence the work reported in this paper.

Data availability

The data that has been used is confidential.

Acknowledgements

This work has been supported by the Research Council of Norway and the industry company partners through the HyLINE project (294739).

References

[1] European Comission, A hydrogen strategy for a climate-neutral Europe, 2020.
[2] C. Yang, J. Ogden, Determining the lowest-cost hydrogen delivery mode, Int. J. of Hydrog. Energy 32 (2) (2007) 268–286.
[3] J.R. Fekete, J.W. Sowards, R.L. Amaro, Economic impact of applying high strength steels in hydrogen gas pipelines, Int. J. of Hydrog, Int. J. of Hydrog. Energy 40 (33) (2015) 10547–10558.
[4] S. Cerniauskas, A.J.C. Junco, T. Grube, M. Robinius, D. Stolten, Options of natural gas pipeline reassignment for hydrogen: cost assessment for a Germany case study, Int. J. of Hydrog. Energy 45 (21) (2020) 12095–12107.
[5] W.H. Johnson, On Some, Remarkable changes produced in iron and steel by the action of hydrogen and acids, Proc. R. Soc. Lond. 23 (156–163) (1874) 168–179.
[6] N.E. Nanninga, Y.S. Levy, E.S. Drexler, R.T. Condon, A.E. Stevenson, A.J. Slifka, Comparison of hydrogen embrittlement in three pipeline steels in high pressure gaseous hydrogen environments, Corros. Sci. 59 (2012).
[7] A. Turnbull, 4 - Hydrogen diffusion and trapping in metals, in: R.P. Gangloff, B. P. Somerday (Eds.), Gaseous Hydrogen Embrittlement of Materials in Energy Technologies 1, Woodhead publishing series in metals and surface engineering, 2012, pp. 89–128.
[8] S. Lynch, Hydrogen embrittlement phenomena and mechanisms, Corros. Rev. 30 (3) (2012) 105–123.
[9] S. Zhang, J. Li, T. An, S. Zheng, K. Yang, L. Lv, C. Xie, L. Chen, L. Zhange, Investigating the influence mechanism of hydrogen partial pressure on fracture toughness and fatigue life by in-situ hydrogen permeation, Int. J. Hydrog. Energy 46 (39) (2021) 20621–20629.
[10] T. Zhang, W. Zhao, Y. Zhao, K. Ouyang, Q. Deng, Y. Wang, W. Jiang, Effects of surface oxide films on hydrogen permeation and susceptibility to embrittlement of X80 steel under hydrogen atmosphere, Int. J. of Hydrog. Energy 43 (6) (2018) 3353–3365.
[11] P. Castaño Rivera, V.P. Ramunni, P. Bruzzoni, Hydrogen trapping in an API 5L X60 steel, Corros. Sci. 54 (2012) 106–118.
[12] I. Moro, L. Briottet, P. Lemoine, E. Andrieu, C. Blanc, G. Odemer, J. Chêne, F. Jambon, Damage under high pressure hydrogen environment of a high strength pipline steel X80. Effects of Hydrogen on Materials, ASM International, 2008, pp. 357–364.
[13] K. Xu, M. Rana, Tensile and fracture properties of carbon and low alloy steels in high pressure hydrogen. Effects of Hydrogen on Materials, ASM International, 2008.
[14] D. Stalheim, T. Boggess, C. San Marchi, S. Jansto, B. Somerday, G. Muralidharan, & P. Sofronis, Microstructure and Mechanical Property Performance of Commercial Grade API Pipeline Steels in High Pressure Gaseous Hydrogen. Proceedings of the 2010 8th International Pipeline Conference, ASME, Volume 2, pp. 529–537, 2010.
[15] T. An, H. Peng, P. Bai, S. Zheng, X. Wen, L. Zhang, Influence of hydrogen pressure on fatigue properties of X80 pipeline steel, Int. J. Hydrog. Energy 42 (23) (2017).
[16] E.S. Drexler, A.J. Slifka, R.L. Amaro, N. Barbosa, D.S. Lauria, L.E. Hayden, D. G. Stalheim, Fatigue crack growth rates of API X70 pipeline steel in a pressurized hydrogen gas environment, Fatigue Fract. Eng. Mater. Struct. 37 (2014).
[17] G.B. Rawls, T. Adams, N.L. Newhouse, 1 - Hydrogen production and containment, in: P.R. Gangloff, B.P. Somerday (Eds.), Gaseous hydrogen embrittlement of materials in energy technologies 2, Woodhead publishing series in metals and surface engineering, 2012.
[18] A. Atrens, D. Mezzanotte, N.F. Fiore, M.A. Genshaw, Electrochemical studies of hydrogen diffusion and permeability in Ni, Corros. Sci. 20 (5) (1980) 673–684.
[19] Q. Liu, A.D. Atrens, Z. Shi, K. Verbeken, A. Atrens, Determination of the hydrogen fugacity during electrolytic charging of steel, Corros. Sci. 87 (2014) 239–258.
[20] C. San Marchi, B. Somerday, S. Robinson, Permeability, solubility and diffusivity of hydrogen isotopes in stainless steels at high gas pressures, Int. J. of Hydrog. Energy 32 (1) (2007) 100–116.
[21] J. Venezuela, E. Gray, Q. Liu, Q. Zhou, C. Tapia-Bastidas, M. Zhang, A. Atrens, Equivalent hydrogen fugacity during electrochemical charging of some martensitic advanced high-strength steels, Corros. Sci. 127 (2017) 45–58.
[22] J. Venezuela, C. Tapia-Bastidas, Q. Zhou, T. Depover, K. Verbeken, E. Gray, Q. Liu, Q. Liu, M. Zhang, A. Atrens, Determination of the equivalent hydrogen fugacity during electrochemical charging of 3.5NiCrMoV steel, Corros. Sci. 132 (2018) 90–106.
[23] Q. Liu, A. Atrens, Z. Shi, K. Verbeken, A. Atrens, Equivalent hydrogen fugacity during electrochemical charging of 980DP steel determined by thermal desorption spectroscopy, Adv. Eng. Mater. 20 (1) (2018).

[24] M.A.V. Devanathan, Z. Stachurski, The adsorption and diffusion of electrolytic hydrogen in palladium, Proc. R. Soc. Lond. Ser. A. Math. Phys. Sci. 270 (1340) (1962) 90–102.
[25] A.J. Kumnick, H.H. Johnson, Steady state hydrogen transport through zone refined irons, Metall. Trans. A 6A (1975) 1087–1091.
[26] D. Pérez Escobar, K. Verbeken, L. Duprez, M. Verhaege, Evaluation of hydrogen trapping in high strength steels by thermal desorption spectroscopy, Materials Science & Engineering, A, Struct. Mater.: Prop., Microstruct. Process. 551 (2012) 50–58.
[27] J. Yamabe, T. Awane, S. Matsuoka, Investigation of hydrogen transport behavior of various low-alloy steels with high-pressure hydrogen gas, Int. J. of Hydrog. Energy 40 (34) (2015) 11075–11086.
[28] T. Casanova, J. Crousier, The influence of an oxide layer on hydrogen permeation through steel, Corros. Sci. 38 (9) (1996) 1535–1544.
[29] J. Flis, Changes in hydrogen entry rate and in surface of iron during cathodic polarisation in alkaline solutions, Electrochim. Acta 44 (23) (1999) 3989–3997.
[30] S.M. Charca, O.N.C. Uwakweh, V.S. Agarwala, Hydrogen transport conditions and effects in cathodically polarized AF1410 steel, Metall. Mater. Trans. A 38 (10) (2007) 2389–2399.
[31] D. Pérez Escobar, C. Miñambres, L. Duprez, K. Verbeken, M. Verhaege, Internal and surface damage of multiphase steels and pure iron after electrochemical hydrogen charging, Corros. Sci. 53 (10) (2011) 3166–3176.
[32] M. Cauwels, R. Depraetere, W.D. Waele, S. Hertelé, T. Depover, K. Verbeken, Influence of electrochemical hydrogenation parameters on microstructures prone to hydrogen-induced cracking, J. Nat. Gas. Sci. Eng. 101 (2022), 104533.
[33] A. Laureys, E. Van den Eeckhout, R. Petrov, K. Verbeken, Effect of deformation and charging conditions on crack and blister formation during electrochemical hydrogen charging, Acta Mater. 127 (2017) 192–202.
[34] A. Nagao, N. Ishikawa, S. Takagi, M. Kimura, Hydrogen uptake in steels exposed to high pressure H2 gas, in: B.P. Somerday, Sofronis (Eds.), International hydrogen conference (IHC2016): Materials performance in hydrogen environments, P. ASME Press, 2017.
[35] A.J. Griffiths, A. Turnbull, On the effective diffusivity of hydrogen in low alloy steels, Corros. Sci. 37 (11) (1995) 1879–1881.
[36] ISO 17081:2014 Method of measurement of hydrogen permeation and determination of hydrogen uptake and transport in metals by an electrochemical technique, International Organization for Standardization, 2014,
[37] G.M. Pressouyre, I.M. Bernstein, A quantitative analysis of hydrogen trapping, Metall. Trans. A 9 (11) (1978) 1571–1580.
[38] Practice for Evaluation of Hydrogen Uptake, Permeation, and Transport in Metals by an Electrochemical Technique, ASTM International, 2018.
[39] E. Wu, A Mathematical Treatment of the Electrochemical Method of Hydrogen Permeation and Its Application in Hydrogen Traps and Embrittlement, J. Electrochem. Soc. 134 (1987) 2126.
[40] L. Simoni, T. Falcade, D.C.F. Ferreira, C.E.F. Kwietniewski, An integrated experimental and modeling approach to determine hydrogen diffusion and trapping in a high-strength steel, Int. J. of Hydrog. Energy 46 (50) (2021) 25738–25751.
[41] T. Zakroczymski, Adaptation of the electrochemical permeation technique for studying entry, transport and trapping of hydrogen in metals, Electrochim. Acta 51 (11) (2006) 2261–2266.
[42] T. Zakroczymski, Permeability of iron to hydrogen cathodically generated in 0.1 M NaOH, Scr. Metall. 19 (4) (1985) 521–524.
[43] Q. Liu, A. Atrens, Reversible hydrogen trapping in a 3.5NiCrMoV medium strength steel, Corros. Sci. 96 (2015) 112–120.
[44] E. Fallahmohammadi, F. Bolzoni, L. Lazzari, Measurement of lattice and apparent diffusion coefficient of hydrogen in X65 and F22 pipeline steels, Int. J. Hydrog. Energy 38 (5) (2013) 2531–2543.
[45] P. Manolatos, M. Jerome, J. Galland, Necessity of a palladium coating to ensure hydrogen oxidation during electrochemical permeation measurements on iron, Electrochim. Acta 40 (7) (1995) 867–871.
[46] H. Husby, M. Iannuzzi, R. Johnsen, M. Kappes, A. Barnoush, Effect of nickel on hydrogen permeation in ferritic/pearlitic low alloy steels, Int. J. Hydrog. Energy 43 (7) (2018) 3845–3861.
[47] P. Bruzzoni, Efectos de superficie en la difusión de hidrógeno en hierro y aleaciones ferrosas, Universidad de Buenos Aires, 2003.
[48] P. Bruzzoni, R.M. Carranza, J.R.C. Lacoste, Influence of palladium films on hydrogen gas entry into iron: a study by electrochemical impedance spectroscopy, Int. J. of Hydrog. Energy (2000) 5.
[49] S. Frappart, X. Feaugas, J. Creus, F. Thebault, L. Delattre, H. Marchebois, Study of the hydrogen diffusion and segregation into Fe–C–Mo martensitic HSLA steel using electrochemical permeation test, J. Phys. Chem. Solids 71 (10) (2010) 1467–1479.
[50] K. Kiuchi, R.B. McLellan, The solubility and diffusivity of hydrogen in well-annealed and deformed iron, Acta Metall. 31 (7) (1983) 961–984.
[51] C.K. Gupta, Chemical Metallurgy: Principles and Practice, Wiley-VCH, Weinheim, 2003, p. 273.
[52] A. Turnbull, l. Wright, Hydrogen permeation modelling with generalised boundary conditions at the charging surface, NPL Rep. Mat. 69 (2014).
[53] P. Delahay, M. Pourbaix, P.V. Rysselberghe, Potential-pH diagrams, J. Chem. Educ. (1950).
[54] J.O. Bockris, J. McBreen, L. Nanis, The Hydrogen evolution kinetics and hydrogen entry into a-iron, J. Electrochem. Soc.. 112 (10) (1965) 1025.
[55] J.O. Bockris, P.K. Subramanyan, The equivalent pressure of molecular hydrogen in cavities within metals in terms of the overpotential developed during the evolution of hydrogen, Electrochim. Acta 16 (12) (1971) 2169–2179.
[56] N. Boes, H. Züchner, Electrochemical methods for studying diffusion, permeation and solubility of hydrogen in metals, J. Less Common Met. 49 (1976) 223–240.
[57] R.B. Hutchings, D.H. Ferriss, A. Turnbull, Ratio of specimen thickness to detection area for reliable hydrogen permeation measurement, NPL Rep. DMM 1 (1993) 103.
[58] T. Zhang, W. Xhao, E. Li, Y. Zhao, Q. Deng, Y. Wang, W. Jiang, Comparison of hydrogen embrittlement susceptibility of three cathodic protected subsea pipeline steels from a point of view of hydrogen permeation, Corros. Sci. 131 (2018) 104–115.
[59] K. Verbeken, 2 - Analysing hydrogen in metals: bulk thermal desorption spectroscopy (TDS) methods, in: R.P. Gangloff, B.P. Somerday (Eds.), (eds)., Gaseous Hydrogen Embrittlement of Materials in Energy Technologies, vol. 1, Woodhead Publishing, 2012, pp. 27–55.
[60] J.-L. Crolet, G. Maisonneuve, Construction of a universal scale of severity for hydrogen cracking, CORROSION 2000, OnePetro, 2000.